

Longitudinal Wake Fields and Chromatic Spot-Size Dilution in the NLC Final Focus

Tor Raubenheimer and Frank Zimmermann

September 25, 1996

1 Introduction

In this note, we evaluate the impact of longitudinal wake fields on the performance of the NLC final focus, and we derive some requirements that these wake fields impose on the beam-pipe aperture, on collimator tapers, and, indirectly, on the machine-protection strategy. Both resistive-wall and geometric wake fields generate an intra-bunch energy spread, which can impair the chromatic correction of the final-focus system and, thereby, cause an increase of the vertical spot size at the interaction point (IP). A similar chromatic dilution also arises from longitudinal space charge, which we have studied for three different final foci in Refs. [1, 2].

The primary effect of the longitudinal wake fields in the final focus is to degrade the chromatic correction of the final doublet. Thus, we are concerned with wake fields between the sextupoles in the chromatic correction section (CCS) and the final doublet. Furthermore: since chromaticity in the vertical plane is substantially larger than that in the horizontal (more than $10\times$), we will only consider effects in the vertical.

The wake fields change both the average bunch energy and the energy spread within the bunch. While the effect of the average energy change can be corrected by appropriately scaling the magnets, the chromatic spot-size increase due to an additional uncorrelated energy spread is in general irrecoverable. Although the energy deviation introduced by both the longitudinal resistive wall and the longitudinal geometric wake fields is actually correlated

with position along the bunch, the variation is very high frequency $\sim \sigma_z$ and thus is extremely difficult to compensate. In the following, we will ignore the possibility of compensating the effect of the induced energy spread.

An energy spread $(\Delta\delta)_{rms}$ arising from wake fields between the sextupoles and the final doublet causes an increase of the IP spot size by

$$\Delta\sigma_y = \xi (\Delta\delta)_{rms} \sigma_{y0} \quad (1)$$

where σ_{y0} is the nominal vertical spot size ($\sigma_{y0} \approx 4-8$ nm), and the dimensionless number ξ characterizes the vertical chromaticity of the final doublet, which for the NLC-Ia and NLC-IIa designs is $\xi \approx 32,000$. The term $\Delta\sigma_y$ has to be added in quadrature to the design spot size.

Using the NLC parameters: the IP spot size increases by 2% for an induced rms energy spread of

$$(\Delta\delta)_{rms,max} \approx 6 \times 10^{-6}. \quad (2)$$

In the following, we assume this value to be the maximum allowed total energy variation induced between the vertical sextupoles and the final quadrupoles. As a point of reference: for a bunch population of 10^{10} the rms energy spread caused by the space charge force is only $(\Delta\delta)_{rms}^{s.c.} \approx 2.5 \times 10^{-8}$ [1, 2], and still negligible.

We will adopt as a design criterion for the NLC final focus that both geometric and resistive-wall wake fields do not give rise to more than half the maximum allowed energy spread each (i.e., 3×10^{-6}), so that the total spot-size dilution from the two types of wake fields is less than 2%.

2 Resistive- Wall Wake Fields

The resistive wall wake fields have been calculated by numerous authors [3]. In the NLC, the bunch length is usually long compared to the characteristic length s_0 which is defined as

$$s_0 = \left(\frac{cb^2}{2\pi\sigma_c} \right)^{1/3} \quad (\text{cgs units}) , \quad (3)$$

where b is chamber radius, c is the speed of light, and σ_c is the conductivity. For example, assuming an aluminum vacuum chamber ($\sigma_c \approx 3.2 \times 10^{17} \text{ s}^{-1}$)

with a 1 cm radius, $s_0 = 25 \mu\text{m}$. This is substantially shorter than the bunch length of $\sigma_z \sim 100\text{--}150 \mu\text{m}$.

In this regime, where the bunch is long compared to the characteristic length s_0 , and assuming a constant conductivity, i.e. the frequency dependence of the conductivity is ignored, the field along a Gaussian bunch can be written [4]:

$$E_z(s/\sigma_z) = \frac{Ne}{4b^2} \left(\frac{s_0}{\sigma_z} \right) f(s/\sigma_z) \quad (\text{cgs units}), \quad (4)$$

where N is the number of particles and

$$f(u) = |u|^{3/2} \exp^{-u^2/4} \left[I_{1/4} \left(\frac{u^2}{4} \right) - I_{-3/4} \left(\frac{u^2}{4} \right) \mp I_{-1/4} \left(\frac{u^2}{4} \right) \pm I_{3/4} \left(\frac{u^2}{4} \right) \right], \quad (5)$$

Here: I are the modified Bessel functions and upper signs are evaluated when $u < 0$ while the lower signs are evaluated when $u > 0$.

For values of $\sigma_z/s_0 \sim 5$, similar to that in the NLC, the function $f(u)$ has a minimum of about -0.5 slightly in front of the bunch center and a maximum of about 0.25 around $2\sigma_z$ towards the bunch tail. The average change in energy is given by:

$$\frac{dE}{ds} = 0.195 \frac{Ne^2}{b^2} \left(\frac{s_0}{\sigma_z} \right)^{3/2} \quad (\text{cgs units}) \quad (6)$$

while the change in rms energy spread is:

$$\frac{d\sigma_E}{ds} = 0.205 \frac{Ne^2}{b^2} \left(\frac{s_0}{\sigma_z} \right)^{3/2} \quad (\text{cgs units}). \quad (7)$$

Assuming aluminum, this can be written in more practical units as

$$(\Delta\delta)_{rms} = 0.036 \frac{N[10^{10}]}{E[\text{eV}] b[\text{cm}] (\sigma_z[\text{cm}])^{3/2}} \Delta s[\text{cm}] \quad (8)$$

where Δs is the length of the beamline or beamline segment considered.

As the bunch length approaches the characteristic length s_0 , the wake field changes character [5, 6]. Regardless, the rms values listed in Eqs. (7) and (8) are still a good approximation for bunch lengths greater than or equal to s_0 . For significantly shorter bunches: our expressions over-estimate the rms energy spread.

In the NLC final focus, the last CCY chromatic correction sextupole is about 400 meters from the final doublet. The vacuum chamber radius has been specified to be 1 cm through the first 200 meters of this distance and 1.5 cm for the second 200 meters-see Chapter 11 in Ref. [11]. In this case, the energy spread from the resistive wall wake field due to an AZ chamber would be roughly $(\Delta\delta)_{rms} = 3.1 \times 10^{-6}$ for a 250 GeV beam with $N = 0.65 \times 10^{10}$ and a bunch length of 100 μm (collider option NLC-Ia) and $(\Delta\delta)_{rms} = 1.4 \times 10^{-6}$ for a 500 GeV beam with $N = 1.1 \times 10^{10}$ and a bunch length of 150 μm (collider option NLC-IIb). This is below or comparable to the tolerance and should not present a limitation.

If instead one considered using a stainless steel vacuum chamber, where the conductivity decreases by at least a factor of 20, we would estimate an induced energy spread of $(\Delta\delta)_{rms} = 13.9 \times 10^{-6}$ for the NLC-Ia parameters and $(\Delta\delta)_{rms} = 6.3 \times 10^{-6}$ for the NLC-IIb parameters. In these cases, the wake field is important. Of course: in this limit, the bunch length is approaching or exceeding the characteristic length and this simple analysis over-estimates the effect. For the NLC-Ia parameters, where the bunch length is roughly equal to the characteristic length, our estimate is about 20% higher than if one correctly accounts for the high frequency fields.

To verify the effect in the NLC final focus, we have modified the 6-D tracking in MAD to include the resistive wall wake field. The short range wake field, assuming a constant conductivity, is given by [5]:

$$E_z(\tilde{s}) = -\frac{Ne}{b^2} \left(\frac{16}{3} \exp^{-\tilde{s}} \cos(\sqrt{3}\tilde{s}) - \frac{16\sqrt{2}}{\pi} \int_0^\infty \frac{dx x^2 \exp^{-x^2\tilde{s}}}{x^6 + 8} \right), \quad (9)$$

where $\tilde{s} = s/s_0$. To simplify the calculation in the tracking, we have approximated the integral in the wake field with an expression that gives the correct asymptotic behavior, has the correct value at $\tilde{s} = 0$, and models the integral well. Thus: MAD uses a wake field:

$$E_z(\tilde{s}) = -\frac{Ne}{b^2} \left(\frac{16}{3} \exp^{-\tilde{s}} \cos(\sqrt{3}\tilde{s}) - \frac{1}{\sqrt{2\pi}} \frac{1}{(a^\alpha + \tilde{s}^{\alpha 3/2})^{1/\alpha}} \right), \quad (10)$$

where $a = 3/4\sqrt{2\pi}$ to give the correct value at $\tilde{s} = 0$ and $\alpha = 0.9$ to give a good approximation to the wake field; a comparison between the full expression and the MAD approximation is shown in Fig. 1.

We have tracked the NLC final focus using this wake field. As expected, we find a component that is added in quadrature to the beam size which scales

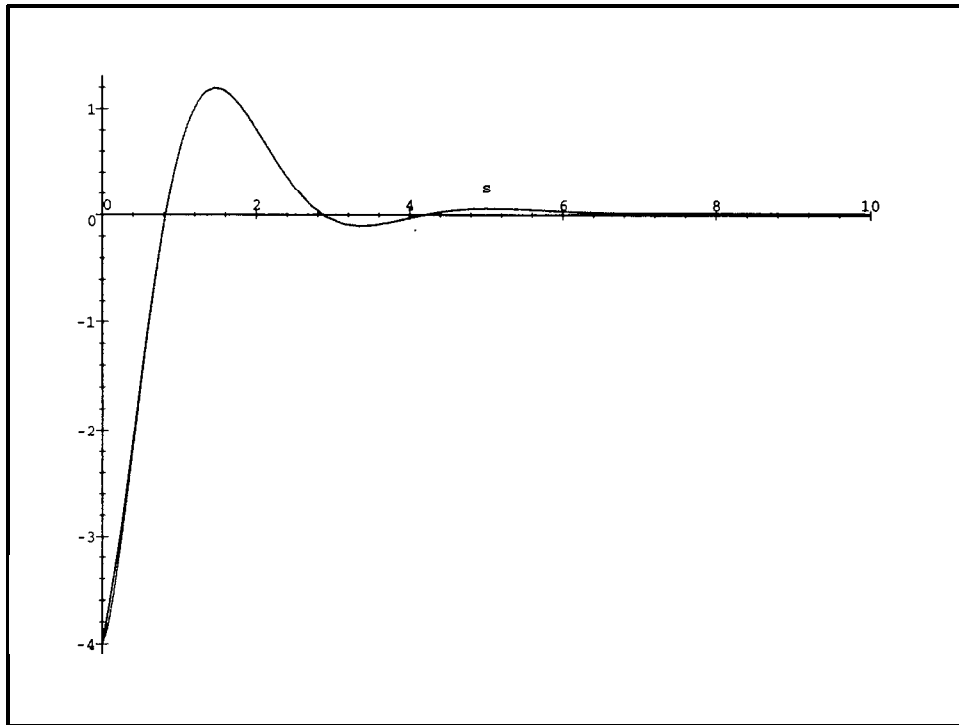


Figure 1: Comparison between the complete expression for the longitudinal resistive wall wake field-Eq. (9)-(dashes) and the approximation that is used in our version of the tracking code MAD-Eq. (10)—(solid). The difference between the exact formula and our approximation is almost invisible.

linearly with beam intensity. For the NLC-IIb parameters with a stainless steel vacuum chamber, we find a contribution of $\Delta\sigma_y = 0.52$ nm, which adds in quadrature to the IP spot size. This is a 1% effect which is roughly a factor of two smaller than our estimate which is partially due to the lower chromaticity of the NLC-IIb lattice. For the NLC-Ia parameters, again with a stainless steel vacuum chamber, we find a component of $\Delta\sigma_y = 1.5$ nm that adds in quadrature to the IP spot size. This is a 5% increase in the beam size which is consistent with our estimate.

Finally, it should be noted that, in practice, there is little reason to constrain the aperture of the chamber except at the quadrupole and sextupole magnets. In fact, the MPS protection method that is outlined suggests that the vacuum chamber would be increased by a factor of three—see Chapter 9 of Ref. [11]. Of course: this implies large transitions which can introduce significant geometric wake fields and is the subject of the next section.

3 Geometric Wake Fields

Similar to the resistive-wall wake fields, also geometric wake fields induce an energy variation $(\Delta\delta)_{rms}$ across the bunch, which could impair the chromatic correction of the final-focus system. Geometric wake fields arise due to changes of the beam-pipe cross section. In the NLC final focus, the primary sources of geometric wake fields are hundreds of proposed protection collimators as well as the changing beam-pipe dimensions around the magnets.

In this section, we will, first: present formulae for the size of the energy variation induced by changes in the beam-pipe cross section and, then, give some numerical estimates of the effect for the NLC final focus. We finally discuss possible implications of our results on the beam-pipe layout in the final-focus system and on the machine-protection strategy.

3.1 Analytical Formulae

If the bunch length is much smaller than the aperture: as is the case in the NLC final focus, the geometric wake field is determined by the high-frequency impedance. For a step-out transition in the beam-pipe cross section, this impedance has been calculated independently by Balakin and Novokhatsky

[7], by Kheifets [8] and by Palumbo [9]. It is

$$Z_{step}^{\parallel} = \frac{Z_0}{\pi} \ln \frac{b}{a} \quad (11)$$

where a and b denote the beam pipe radius before and after the transition step, and Z_0 is the vacuum impedance. The imaginary part of the impedance vanishes as $1/\gamma^2$ [9]. The same formula: Eq. (11), applies to an untapered collimator, consisting of a step-in followed by a step-out. The reason is that the beam loses almost no energy at the step-in, because: for the step-in, the radiated energy is approximately canceled the positive change in the synchronous field energy [8].

The longitudinal wake function of a step-out or untapered collimator is obtained from the impedance in Eq. (11) via Fourier transform:

$$W_0(s) = \frac{2}{\pi} \int_0^{\infty} d\omega \operatorname{Re} Z^{\parallel}(\omega) \cos \frac{\omega s}{c} \quad (12)$$

The impedance (11) is independent of frequency, and in this case the wake function is a delta function:

$$W_{0,step}(s) = \frac{2cZ_0}{\pi} \ln \frac{b}{a} \delta(s) \quad (13)$$

For a Gaussian bunch of N particles, the average and rms relative energy change due to an untapered step-out is then

$$(\Delta\delta)_{ave}^{step} = \frac{2Nr_e}{\sqrt{\pi}\gamma\sigma_z} \ln \frac{b}{a} \approx 1.13 \times \frac{Nr_e}{\gamma\sigma_z} \ln \frac{b}{a} \quad (14)$$

$$(\Delta\delta)_{rms}^{step} = \left(\frac{1}{\sqrt{3}} - \frac{1}{2} \right)^{\frac{1}{2}} \frac{4Nr_e}{\sqrt{2\pi}\gamma\sigma_z} \ln \frac{b}{a} \approx 0.444 \times \frac{Nr_e}{\gamma\sigma_z} \ln \frac{b}{a} \quad (15)$$

where r_e is the classical electron radius, γ the energy in units of the rest energy: σ_z denotes the rms bunch length, and we have assumed a Gaussian beam profile. Notice that the energy change only depends on the beam-pipe radius and the bunch length: and neither on the beam size nor the beta function.

If there is no abrupt step transition, but the beam-pipe radius is gradually tapered, the energy loss due to a collimator can be greatly reduced. In

Ref. [10], Heifets and Kheifets have shown that, for a double-sided tapered transition in the high-frequency limit, the longitudinal loss factor is given by

$$(\Delta\delta)_{ave}^{taper} = \frac{2Nr_e}{\sqrt{\pi}\gamma\sigma_z} (1 - \tilde{\eta}_1) \ln \frac{b}{a} \approx 1.13 \times \frac{Nr_e}{\gamma\sigma_z} (1 - \tilde{\eta}_1) \ln \frac{b}{a} \quad (16)$$

where $\tilde{\eta}_1 = \min(1.0, \eta_1)$ with

$$\eta_1 \equiv \frac{g\sigma_z}{(b-a)^2} \approx \frac{\sigma_z}{\alpha(b-a)}. \quad (17)$$

Here, g is the length of the taper, and $\alpha = \arctan((b-a)/g) \approx (b-a)/g$ the taper angle with respect to the beam direction. The rms energy variation is

$$(\Delta\delta)_{rms}^{taper} = 0.444 \times \frac{Nr_e}{\gamma\sigma_z} (1 - \tilde{\eta}_1) \ln \frac{b}{a}. \quad (18)$$

If the taper is sufficiently shallow, $\tilde{\eta}_1 = 1$ and there is no energy loss.

The energy spread induced by a flat collimator, is, up to a numerical factor of order one, given by the same formulae, when the beam-pipe radius a is replaced by the collimator half gap.

If there are very many narrowly spaced transitions, the electromagnetic waves generated at different transitions can interfere, and the above formulae need to be modified in order to account for this interference. For the special case of a periodic array of M cavities and $A4 \gg \omega a^2/(cL)$ —here a denotes the iris radius and L the longitudinal period—, Heifets and Kheifets [10] have calculated the real part of the high-frequency impedance as

$$\text{Re}Z^{\parallel} = \frac{2Z_0c^{3/2}}{(\omega a)^{3/2}} \left(\frac{2L}{\pi a}\right)^2 \left(\frac{\pi a}{g}\right)^{\frac{1}{2}}, \quad (19)$$

where g denotes the cavity gap.

For a variety of reasons formula (19) is not applicable to our problem: First, the positions of collimators and transitions in the final focus do not follow a periodic pattern. Second, the changes in beam-pipe radius are typically so small that $2\sigma_z g/(b-a)^2 \geq 1$, g being the distance between two adjacent collimators, which means the widened spaces between collimators do not resemble cavities, but the transitions are really more like steps. Third, Eq. (19) only describes the high-frequency impedance, and, since the latter decreases as $\omega^{-3/2}$, the loss factor depends on the low-frequency range of the impedance and is uncertain.

In the next section, we will use Eqs. (15) and (18) to estimate the rms energy variation induced by a single untapered or tapered transition, respectively, and we will simply sum the effects of individual transitions, thereby neglecting interference effects.

3.2 Numerical Estimates for the Final Focus'

The passive machine protection philosophy outlined in the Chapters 9 and 16 of the Zeroth Order Design Report (ZDR) [11], advocates the installation of a protection collimator in front of each quadrupole and each bending magnet. The inner apertures of the final-focus magnets are about 10 mm in radius. The protection collimators are suggested to be a factor 2-3 narrower (4-5 mm radius), while the beam-pipe radius in between is thought to be a factor of 3 larger than the magnet openings (30 mm) [11].

From the entrance to the vertical chromatic correction section (CCY) to the IP, the NLC final focus accommodates roughly 200 bending magnets, quadrupoles and sextupoles. If we assume that each of these magnets is passively protected by its own upstream protection collimator, we expect about 400 step-out transitions in the beam pipe cross section: 200 from 4.5 mm to 30 mm, and 200 from 10 mm to 30 mm (as mentioned; abrupt step-in transitions should not contribute to the beam energy loss).

In the following, to make a conservative estimate of the wake-field effects, we consider the 500-GeV c.m. collider version NLC-I ($\gamma \approx 5 \times 10^5$), since the wake fields are more critical at lower energy. Pessimistically assuming 10^{10} particles per bunch and an rms bunch length of 100 μm , Eq. (15) predicts an induced relative rms energy spread of

$$(\Delta\delta)_{rms} \approx 2.7 \times 10^{-7} \quad \text{for a step-out from 10 to 30 mm} \quad (20)$$

$$(\Delta\delta)_{rms} \approx 4.7 \times 10^{-7} \quad \text{for a step-out from 4.5 to 30 mm} \quad (21)$$

if the transitions are abrupt and untapered. The energy changes suffered at different locations add linearly, since the wake function is always of the same shape. Then, the total induced rms energy variation is determined to be as large as 1.5×10^{-4} , 25 times larger than our tolerance: and it would increase the IP spot size by a factor of 5!

This has three possible implications: First, one could drastically reduce the number of protection collimators; the assumed number of 200 seems a little excessive in any case. Suppose we only have one protection collimator

and one further change of the beam-pipe cross section for every 5 magnets, then the spot-size increase is still a considerable 41%. An acceptable 1% increase is obtained, if there are only six beam-pipe transitions and four protection collimators in the entire system (one collimator for every 50 magnets; this would correspond to a total number of collimators equal to 6, since there are also 2 primary collimators in the CCY, which we will comment on later).

Second, one could taper all the collimators and beam-pipe transitions. From Eq. (17), the energy loss of a symmetrically tapered collimator or transition vanishes: if the single-taper length is larger than 4 and 6.5 m, respectively.

Then, for 200 collimators and 200 additional beam-pipe transitions, the combined length of all tapers would be 4.4 km, which would quadruple the present length of the final-focus system! The tapers cannot be chosen much shorter than what we have assumed. For instance, if they are half as long, the wake effect would only be reduced by a factor of 2 compared with that from an untapered collimator or transition, and this would not be sufficient.

Finally, we briefly consider the wake effect from the two main vertical collimators in the final focus. These collimators will be installed close to the sextupoles in the vertical chromatic correction section, and their purpose is to perform a second, clean-up, collimation of the final-doublet betatron phase. (The primary collimation of this phase takes place upstream of the big bend.)

Assuming a normalized vertical emittance of $\gamma\epsilon_y \approx 7 \times 10^{-9}$ m, and a beta function at the vertical sextupoles of $\beta_y \approx 200$ km, the vertical beam size at this collimator pair is $\sigma_y \approx 170 \mu\text{m}$. Thus, for the design collimation depth of $40 \sigma_y$, the collimator aperture is about a ≈ 6.7 mm. This aperture is similar to (or even somewhat larger than) that assumed above for the protection collimators; hence: the wake effect of the main collimators is of comparable magnitude. Since there are only two of these collimators, this would be quite acceptable.

4 Conclusions

Chromatic dilution of the IP spot size places a limit on the maximum tolerable intra-bunch energy spread induced by final-focus wake fields. In this paper: we have evaluated the energy spread arising from both resistive-wall and geometric wake fields.

For the resistive-wall wakes, we find that there is little effect from an aluminum vacuum chamber, but the spot size increase can be significant, if a material with higher resistivity is utilized. In particular, assuming that the vacuum chamber has a 1.5 cm radius for the first 200 meters from the IP and then a 1 cm radius for the next 200 meters to the CCY, the NLC-Ia spot size is increased by 5% if the vacuum chamber is made from stainless steel, for which the resistivity is twenty times higher than for aluminum. Of course, if the chamber radius is increased: the dilution will decrease; the induced energy spread scales inversely with the chamber radius.

Our study of geometric wake fields shows that the longitudinal wake fields arising from the two main collimators in the CCY alone would cause a spot-size increase of 0.01%, which is negligible.

However, the current machine protection philosophy for the NLC final focus envisions a few hundred magnet protection collimators and transitions between different beam-pipe radii in the range 5-30 mm. The combined effect of the geometric wake fields from all these collimators and transitions, if untapered, would cause a fivefold increase of the IP spot size. To render the wake-field effect unimportant, the collimators: and other transitions, must be tapered on either side. Since the typical single-taper lengths required are of the order 4-7 m, the combined length of all tapers would exceed 4 km, which could quadruple the length of the final-focus system. This appears highly impractical: and we, therefore: recommend a revision of the machine-protection strategy for the NLC final focus.

References

- [1] F. Zimmermann and T.O. Raubenheimer, "Longitudinal Space Charge in the SLC, FFTB and NLC Final-Focus Systems", to be published in the Proceedings of the *5th European Particle Accelerator Conference (EPAC 96)*, Sitges, Barcelona, Spain, 10 – 14 June, 1996, *SLAC-PUB-7139* (1996).
- [2] F. Zimmermann and T.O. Raubenheimer, "Longitudinal Space Charge in Final-Focus Systems for Linear Colliders", submitted to *Physical Review E*, and *SLAC-PUB-7304* (1996).

- [3] For a detailed list of references see: A. Chao, *Physics of Collective Beam Instabilities in High Energy Accelerators*, John Wiley & Sons, New York, NY (1993).
- [4] A. Piwinski, DESY Report 72/72 (1972).
- [5] K.L.F. Bane, “The Short Range Resistive Wall Wakefields,” SLAC AP-87 (1991).
- [6] O. Henry and O. Napoly, “The Resistive-pipe Potentials for Short Bunches,” *Part. Acc.*, **35**:235 (1991).
- [7] V.E. Balakin and A.V. Novokhatski, Proc. 12-th Int. Conf. High Energy Accel., Batavia, 1984, p.117 (1984).
- [8] S.A. Kheifets, IEEE Trans. Microwave Theory Technique MTT-35, 753-760 (1987).
- [9] L. Palumbo, “Analytical Calculation of the Impedance of a Discontinuity” , *Particle Accelerators* 25, pp. 201-216 (1990).
- [10] S.A. Heifets and S.A. Kheifets, “Coupling Impedance in Modern Accelerators” , *Rev. Mod. Phys.*, Vol. 63, No. 3 (1991).
- [11] The NLC Design Group, “Zeroth Order Design Report for the Next Linear Collider” , Chapters 9 and 16, in particular Section 9.2.2 (pp. 569): *LBNL-5424, SLAC-474, UCRL-ID-124161, UC-414* (1996).